# Photoelectrochemical hybrid cell for unbiased $CO_2$ reduction coupled to alcohol oxidation

Daniel Antón-García[a], Esther Edwardes Moore[a], Mark A. Bajada[a], Annika Eisenschmidt[a], Ana R. Oliveira[b], Inês A. C. Pereira[b], Julien Warnan*[c] and Erwin Reisner*[a]

Corresponding authors:

Julien Warnan (julien.warnan@tum.de)

Erwin Reisner (reisner@ch.cam.ac.uk)

[a] Yusuf Hamied Department of Chemistry, University of Cambridge, Lensfield Road, Cambridge CB2 1EW, United Kingdom

[b] Instituto de Tecnologia Química e Biológica António Xavier, Universidade Nova de Lisboa, Av. da República, 2780-157 Oeiras, Portugal

[c] Chemistry Department, Technische Universität München, Lichtenbergstraße 4, 85747 Garching, Germany

**Abstract**

The reduction of $CO_2$ to renewable fuels must be coupled to a sustainable oxidation process to devise a viable solar fuel-producing device. In photoelectrochemical cells, water oxidation to $O_2$ is the predominant oxidation reaction and typically requires a pair of light absorbers or an applied bias voltage when coupled to $CO_2$ reduction. Here, we report a bias-free photoelectrochemical device for simultaneous $CO_2$ reduction to formate and alcohol oxidation to aldehyde in aqueous conditions. The photoanode is constructed by co-immobilisation of a diketopyrrolopyrrole-based chromophore and a nitroxyl-based alcohol oxidation catalyst on a mesoporous $TiO_2$ scaffold, providing a precious metal-free dye-sensitised photoanode. The photoanode was wired to a biohybrid cathode consisting of the $CO_2$ reduction enzyme formate dehydrogenase integrated into a mesoporous indium tin oxide electrode. The bias-free cell delivers sustained photocurrents of up to 30 μA $cm^{-2}$ under visible-light irradiation, resulting in simultaneous aldehyde and formate production. Our results show that single light absorber photoelectrochemical cells can be used for parallel fuel production and chemical synthesis from $CO_2$ and waste streams in the absence of an external bias.

## Introduction

The reduction of $CO_2$ coupled to water oxidation offers an attractive approach for the production of carbon neutral fuels through a closed redox cycle.[1,2] However, the thermodynamically demanding and kinetically sluggish water oxidation reaction as well as the lack of commercial value for the evolved $O_2$ product, pose a challenge to the technoeconomic viability of this process.[3–5] An alternative oxidation pathway, requiring less thermodynamic driving force, may enable the simultaneous generation of fuels and cost-effective synthesis of valorised chemicals providing a higher opportunity for profitability than the traditional reduction of $CO_2$ coupled to water oxidation.[3,5–7] In particular alcohols, which are readily obtainable from biomass,[8] can be (photo)electrochemically oxidised in aqueous conditions.[9,10] Upgrading biomass through oxidation provides greener routes for aldehyde and ketone synthesis, which can be of importance in the fine chemicals industry.[6,11] To date, the chemical synthesis of value-added products coupled to $CO_2$ reduction has mostly been studied in electrolysers, with a large voltage bias being required to drive the reactions,[12–14] or in colloidal photocatalytic systems using organic solvents.[15,16]

Photoelectrochemical (PEC) cells offer the possibility of employing sunlight to power the electrochemical reactions.[17] Oxidative organic transformations have been recently explored in PEC cells, typically employing heterogenous 'narrow' band gap semiconductors (i.e., $BiVO_4$) as the photoanode.[9,18,19] The reported photoanodes have so far only been coupled to $H_2$-evolving cathodes and typically require an additional electrical bias due to insufficient driving force upon photoexcitation.[10,18] Similarly, an applied bias voltage was provided by an external photovoltaic module to a substrate oxidation photoanode and a $CO_2$-reducing cathode.[20] Furthermore, these semiconductors often suffer from photocorrosion and competing water oxidation in aqueous media, and thus perform best in organic solvents, potentially limiting the environmental compatibility of this approach.[19,21,22] A PEC-only cell capable of bias-free substrate oxidation coupled with $CO_2$ reduction has thus far not been reported.

The lack of stability and tunability of heterogenous materials can be addressed by separating the light absorption, charge separation and transportation properties.[23] Consequently, a dye-sensitised $TiO_2$ photoanode benefits from the fine-tuning of a molecular chromophore, as well

as from the stability and high dielectric permittivity of the $TiO_2$ semiconductor (SC), which possesses a conduction band (CB) with just sufficient potential for $CO_2$ reduction when using an ideal, reversible electrocatalyst.[23,24] However, reports of dye-sensitised photoanodes for alcohol oxidation are scarce, featuring low faradaic efficiency (FE, < 50%) and the use of precious metals.[25–27] In addition, most synthetic catalysts for $CO_2$ reduction require a substantial overpotential and cannot operate with the driving force provided by CB electrons of $TiO_2$.

In this study, we report a single-light absorber PEC cell for bias-free simultaneous substrate oxidation and $CO_2$ reduction (Fig.1a). The precious metal-free cell comprises a organic dye- and catalyst-sensitised $TiO_2$ photoanode for alcohol oxidation, and a biohybrid cathode for $CO_2$ reduction. Two dyes based on a diketopyrrolopyrrole (DPP) core, which has previously been explored for PEC solar fuel production,[28,29] were synthesised, and feature two distinct anchoring groups (carboxylic and phosphonic acid, **DPP-CA** and **DPP-PA** in Fig. 1b). The dyes are co-immobilised with an organic nitroxyl radical alcohol oxidation catalyst, which is functionalised with a silatrane anchor (**STEMPO**, TEMPO = 2,2,6,6-tetramethylpiperidine-*N*-oxyl, Fig. 1b), on a mesoporous $TiO_2$ ($mTiO_2$) scaffold.[6,10,14] Comparison with a ruthenium-based chromophore (**RuP**, $[Ru(bpy)_2((4,4'\text{-}(OH)_2PO)_2bpy)]Br_2$, (4,4′-$(OH)_2PO)_2$-bpy = 2,2′-bipyridine-4,4′-diyldiphosphonic acid, Fig. 1b), typically used as a benchmark in dye-sensitised photoanodes and colloids,[25,30] showcases the advantages of organic sensitisers. The resulting photoanode was subsequently wired to a semi-artificial $CO_2$ reduction cathode with a W-containing formate dehydrogenase (FDH) enzyme on a mesoporous indium tin oxide electrode (mITO) capable of direct electron transfer (Fig. 1a). mITO provides a biocompatible electrode material for the wiring of fuel-forming enzymes,[31,32] and FDH serves as an ideal bioelectrocatalyst for $CO_2$ reduction due to its high activity and selectivity for formate production close to the thermodynamic potential.[32,33] Visible light irradiation of the two-electrode PEC cell photoinduces an electron transfer cascade (Fig. 1a) starting from the excited dye, through the $mTiO_2$, to the mITO and thence to the FDH which ultimately reacts with $CO_2$. Simultaneously, hole transfer from the oxidised dye to the neighbouring **STEMPO** triggers alcohol oxidation. Our two-electrode PEC cell is capable of sustaining photocurrents over the six-hour experiment, resulting in quantifiable formate and aldehyde (4-methylbenzaldehyde (4-MBAd) or

2,5-diformylfuran (DFF) from 4-methylbenzylalcohol (4-MBA) or 5-hydromethylfuran (HMF), respectively) under bias-free conditions.

## Results and Discussion

### Dye synthesis and characterisation

Synthesis of both organic chromophores (Fig. 2a) started with reaction of **DPP$_{Br}$**[34] with phenylboronic acid to yield **DPP$_{Ph}$** in 77% yield. Condensation in the presence of piperidine with either cyanoacetic acid or diethyl cyanomethylphosphonate yielded **DPP-CA** (68%) or **DPP-PA$_{Et}$** (75%), respectively. Deprotection of the phosphonic acid was achieved by reflux in chloroform solution in the presence of bromotrimethylsilane (TMSBr), followed by hydrolysis with methanol (MeOH) affording **DPP-PA** in 80% yield. The composition and purity of the dyes were confirmed by $^{1}$H, $^{13}$C and $^{31}$P NMR spectroscopy (Supplementary Figure 1−6), high-resolution mass spectrometry, infrared spectroscopy, and elemental analysis.

The UV-vis absorption spectra of **DPP-CA** and **DPP-PA** were recorded in *N*,*N*-dimethylformamide (DMF) solution (Fig. 2b), with both chromophores featuring a maximum absorption band at $\lambda_{max}$ = 498 nm ($\varepsilon_{max}$ = 25.7 mM$^{-1}$ cm$^{-1}$) and $\lambda_{max}$ = 502 nm ($\varepsilon_{max}$ = 14.1 mM$^{-1}$ cm$^{-1}$), respectively. **RuP** features a weaker light absorption ($\varepsilon_{max}$ = 11.0 mM$^{-1}$ cm$^{-1}$) centred at shorter wavelengths ($\lambda_{max}$ = 457 nm). Fluorescence spectra recorded in diluted DMF solution allowed to calculate a zero-zero energy transition ($E_{0-0}$) of ~2.25 eV for both organic dyes (Supplementary Figure 7). Strong colouration of a m$TiO_2$ film (anatase nanoparticles, *ca.* 20 nm diameter, ~6 µm thick) on a glass substrate after immersion in a solution of the dyes confirmed the binding of the molecules to the surface (Supplementary Figure 8).

To gain insight into the electronic structures of **DPP-CA** and **DPP-PA**, geometry optimisations were performed by employing density functional theory (DFT) at the PBE0/6-311G(d,p) level (Supplementary Table 1 and Supplementary Table 2). Subsequent time-dependent DFT (TD-DFT) calculations at the CAM-B3LYP/6311+G(2d,p) level were conducted,[34] with the calculated UV-vis absorption spectra from TD-DFT calculations matching the one experimentally recorded for **DPP-CA** and **DPP-PA** (Supplementary Figure 9). For both

chromophores, the peak at *ca.* 500 nm corresponds mainly to a HOMO to LUMO transition (Supplementary Table 3), originating in the DPP core and extending to the anchoring moiety, suggesting charge density directionality in the excited state (Fig. 2c and Supplementary Figure 10).

The electrochemical properties of **DPP-CA** and **DPP-PA** were studied via cyclic voltammetry (CV) in DMF solution, and chemisorbed on a mITO electrode (particle size < 50 nm, film thickness ~3 µm)[29,35,36] in acetonitrile (MeCN), with tetrabutylammonium tetrafluoroborate ($TBABF_4$) as a supporting electrolyte (Supplementary Figure 11, Supplementary Figure 12 and Supplementary Table 3). Combining the oxidation potentials ($E(D^+/D)$) and $E_{0\text{-}0}$ values enabled estimations of the oxidation potential in the excited state ($E(D^+/D^*)$) for **DPP-CA** and **DPP-PA** at −0.95 and −0.90 V *vs.* the normal hydrogen electrode (NHE), respectively. These values are more negative than the CB of $TiO_2$ ($E_{CB}(TiO_2)$ = −0.57 V *vs.* NHE at pH 7),[24] allowing exergonic electron injection. Secondly, $E(D^+/D)$ of immobilised **DPP-CA** (+1.33 V *vs.* NHE) and **DPP-PA** (+1.28 V *vs.* NHE) is more positive than the onset for alcohol oxidation by **STEMPO** ($E_{onset}$ = +0.75 V *vs.* NHE at pH 7),[14] allowing for hole transfer to the catalyst. The reported values for **RuP** ($E(D^+/D^*)$ = −0.78 V *vs.* NHE and $E(D^+/D)$ = +1.37 V *vs.* NHE)[37] are also favourable for the desired charge transfer events and confirm that all dyes meet the thermodynamic requirements for their incorporation in an alcohol-oxidising photoanode.

**Photoanode assembly**

The photoanodes were prepared by optimised sequential immobilisation of the catalyst, as the kinetic bottleneck,[29,38,39] followed by saturation of the remaining exposed surface by the chromophore to provide high light absorption. Firstly, immobilisation of the catalyst was achieved by immersion of a $mTiO_2$ film (anatase nanoparticles, *ca.* 20 nm diameter, ~6 µm thick) in a solution of **STEMPO** (see Methods for details), resulting in the hydrolysis of the silatrane moiety and formation of strong siloxane bonds with the $TiO_2$.[14] The resulting $mTiO_2$|**STEMPO** electrodes were then immersed in a solution of the dye in dichloromethane (DCM) (0.2 mM **DPP-CA** or **DPP-PA**) or MeOH (0.2 mM **RuP**) to afford the photoelectrodes $mTiO_2$|**STEMPO**/dye (see Methods for details).

We carried out photoanode characterisation via PEC experiments at room temperature in a one-compartment three-electrode cell using a Pt counter electrode, a Ag/AgCl/$KCl_{sat}$ reference electrode and a functionalised m$TiO_2$ film on FTO-coated glass as the working photoelectrode. Linear sweep voltammetry (LSV) and controlled potential photoelectrolysis (CPPE) experiments were performed under chopped light irradiation. UV-filtered simulated solar light (100 mW $cm^{-2}$, AM 1.5G, λ > 420 nm) was used for all PEC measurements, avoiding direct excitation of the $TiO_2$ semiconductor.

Different aqueous electrolytes employing a range of pH values and buffers were first examined in the presence of 4-MBA as a model oxidation substrate using **DPP-CA** (Supplementary Figure 13), **DPP-PA** (Supplementary Figure 14) or **RuP** (Supplementary Figure 15) as photoabsorbers. CPPE experiments were performed for 6 h at an applied potential ($E_{app}$) of +0.4 V *vs.* the reversible hydrogen electrode (RHE), a sufficiently positive potential for efficient extraction of charges from the CB of $TiO_2$ (see above). We monitored oxidation of 4-MBA to 4-MBAd by high-performance liquid chromatography (HPLC) at the end of the CPPE experiments, with all electrolyte solutions enabling high FEs of 80−100% and 60−90% for 4-MBAd formation when employing **DPP-CA** (Supplementary Table 5) or **DPP-PA** (Supplementary Table 6), respectively. No overoxidation product (i.e., 4-methylbenzoic acid) was observed in line with the selectivity of the **STEMPO** catalyst for alcohol substrates.[14] Selection of the optimised electrolyte was performed by comparison of the PEC performance and evaluation of the dye stability, observed by UV-vis spectroscopy of the assembled photoanodes at the end of the CPPE experiment (**DPP-CA**, Supplementary Figure 16; **DPP-PA**, Supplementary Figure 17; **RuP**, Supplementary Figure 18).

Comparison of the dye performances during CPPE under their optimised conditions, i.e., sodium borate ($Na_2B_4O_7$) buffer pH 8.0 for **DPP-CA** and **DPP-PA** and sodium acetate (NaOAc) buffer pH 5.6 for **RuP** (**Error! Reference source not found.**a), reveals a higher activity ($J$ = ∼90 μA $cm^{-2}$) of the organic dyes compared to **RuP** ($J$ = ∼9 μA $cm^{-2}$, Supplementary Table 7). This can be partially explained by the superior light harvesting efficiency (LHE) of the organic dye-based electrodes over **RuP** (Supplementary Figure 19). We focused on **DPP-CA** for further experiments

due to its higher photocurrent activity and FE compared to **DPP-PA**, its maximum LHE ensuring non-limiting light absorption, as well as its versatility in different electrolytes and conditions.

The solvent for **DPP-CA** immobilisation was investigated with higher loading (evaluated by UV-vis) and catalytic activity obtained with DCM (Supplementary Figure 20 and Supplementary Table 8) compared to DMF and MeOH. We then quantified the initial chromophore loading for $mTiO_2$|**DPP-CA** and $mTiO_2$|**STEMPO**/**DPP-CA** electrodes via UV-vis absorption (see Methods for details), revealing loadings of 117 ± 16 and 54 ± 5 nmol $cm^{-2}$, respectively. The catalyst loading on $mTiO_2$|**STEMPO** electrodes was calculated as 176 ± 26 nmol $cm^{-2}$ by inductively coupled plasma optical emission spectrometry (ICP-OES, see Methods for details), resulting in a catalyst/dye ratio of 3.2. The unusually high catalyst loading compared to molecular catalysts on metal oxides (50–100 nmol $cm^{-2}$)[35,40,41] may be attributed to the polymerisation of hydrolytically unstable silatrane moieties on the surface which may not be electrochemically active,[14] thus providing a conservative value when calculating turnover numbers (TON, see Methods for details).

**Performance evaluation**

The LSV of the optimised $mTiO_2$|**STEMPO**/**DPP-CA** electrode (Supplementary Figure 21) displayed photocurrents with an early onset close to the CB of $TiO_2$ ($E_{CB}(TiO_2)$ = −0.16 V *vs.* RHE).[24] A $TON_{\mathbf{STEMPO}}$ of 54 and a $TON_{\mathbf{DPP\text{-}CA}}$ of 351 were achieved by the fully assembled $mTiO_2$|**STEMPO**/**DPP-CA** photoanode over a 6 h CPPE experiment at +0.4 V *vs*. RHE, with a FE of 94%, confirming the catalytic nature of the photoanode with respect to both molecular components (Fig. 3b and Supplementary Table 9).

We further conducted control experiments to confirm that substrate oxidation originated from both **STEMPO** and **DPP-CA** (Fig. 3b and Supplementary Table 9). Dye-free $mTiO_2$|**STEMPO** electrodes led to a negligible photocurrent response, while **STEMPO**-free $mTiO_2$|**DPP-CA** electrodes displayed an initial photocurrent of 36 µA $cm^{-2}$, which rapidly decayed during the CPPE experiment due to the absence of efficient catalytic turnover that results in chromophore decomposition. Immobilisation of TEMPO-free 3-aminopropylsilatrane (**Sil**), followed by immobilisation of **DPP-CA** resulted in a lower dye loading compared to that of $mTiO_2$|**DPP-CA**

electrodes (Supplementary Figure 22), as well as low, rapidly decreasing photocurrents during CPPE. This confirms that the high activity and stability of the fully assembled system stems from the incorporation of the TEMPO moiety, and hence ruling out alternative catalytic activity sources such as lower **DPP-CA** aggregation and alteration of the $TiO_2$ SC by the silatrane moiety.[42,43] Employing the m$TiO_2$|**DPP-CA** system in the presence of solubilised TEMPO (1 mM) in the electrolyte led to 4-MBAd production with high FE (99%). However, limited photocurrents of ~20 μA $cm^{-2}$ with $TON_{TEMPO}$ < 1 were reached, in line with previous reports on TEMPO-mediated dye-sensitised systems[44] and highlighting the benefits of immobilised molecular catalysts on heterogenous scaffolds.[45]

Finally, we recorded the incident photon-to-current efficiency (IPCE, see Supplementary Methods for details) at +0.4 V *vs.* RHE for the fully-assembled system (Supplementary Figure 23) reaching a value of 2% at 425 nm, and reflecting the LHE spectrum of the corresponding m$TiO_2$|**STEMPO**/**DPP-CA** electrodes.

The electrodes retained 50% of their activity after 12 h of irradiation during CPPE, with a sustained drop in activity up to 22 h (**Error! Reference source not found.**c). This compares favourably with organic chromophore-driven photoanodes which have a maximum recorded stability of 1 h.[26,46] At the end of the experiment, the photoanode produced 23 ± 2 μmol $cm^{-2}$ of 4-MBAd, with a high FE of (87 ± 4)%, an absolute yield for the conversion of 4-MBA to 4-MBAd of (6.6 ± 0.3)% (Supplementary Table 10), and $TON_{\mathbf{STEMPO}}$ and $TON_{\mathbf{DPP\text{-}CA}}$ of 131 ± 22 and 853 ± 107, respectively. The maximum TONs obtained are significantly higher than those reported for organic chromophores coupled to Ru-based catalysts on water-oxidising photoanodes, which are consistently below 30.[47,48] Attempts to revive the catalytic activity by immobilising fresh **DPP-CA** on an electrode after the CPPE experiment did not result in significant photocurrents, suggesting **STEMPO** decomposition being the main cause of the activity loss (Supplementary Figure 24).[14]

**Substrate scope**

We replaced the 4-MBA substrate by HMF, a compound of interest as it can be sourced from biomass and its oxidation products are of value as industrially-relevant building blocks.[8]

Photocurrents of 70 μA $cm^{-2}$ were achieved in $Na_2B_4O_7$ buffer (0.1 M, pH 8.0) under the previously optimised conditions (**Error! Reference source not found.**d). We also tested $NaHCO_3$ buffer (0.05 M, pH 6.4) to investigate the compatibility with an FDH-based cathode (see below), resulting in currents of 40 μA $cm^{-2}$. The higher activity in pH 8.0 solution was consistent with higher TEMPO activity at more alkaline pH, resembling the conditions typically used in the literature for its electrochemical oxidation.[6,10] HMF oxidation proceeds through initial alcohol oxidation, which can be followed by further oxidation reactions to form a wide range of products (Supplementary Figure 25).[10,49] HPLC analysis revealed selectivity for DFF, a high-value monomer employed in the polymer industry[8], with no overoxidation products being detected. This may be a consequence of the low overall conversion yield (Supplementary Table 11), and of the experimental conditions, which can impact product selectivity.[50,51] DFF was produced with a FE of 86−90% under both electrolyte conditions (Supplementary Table 11).

**Photoelectrochemical $CO_2$ reduction and chemical synthesis**

To construct the $CO_2$-reducing cathode, we assembled a mITO scaffold (particle size 50 nm, film thickness ~8.5 μm), followed by immobilisation of FDH by drop casting the enzyme onto the electrode surface (274 pmol $cm^{-2}$).[32,52] We selected a W-containing formate dehydrogenase from *D. vulgaris* Hildenborough for its high catalytic activity and ability to reduce $CO_2$ with a marginal overpotential on mITO electrodes.[32]

We evaluated individually the mITO|FDH cathode and m$TiO_2$|**STEMPO**/**DPP-CA** photoanode in a three-electrode configuration in a $CO_2$-saturated $NaHCO_3$ buffered solution (0.05 M, pH 6.4), with 4-MBA present for the photoanode experiment. The voltametric responses on the LSV of both systems reveal a current matching occurring at *ca.* +0.06 V *vs.* RHE (Fig. 4a). CPPE of the assembled photoanode and cathode showed sustained (photo)currents over the course of 6 h resulting in 4-MBAd and formate production with a FE of 113% and 90%, respectively (Supplementary Figure 26 and Supplementary Table 12). The excessively high FE from the photoanode at this applied potential is attributed to inefficient electron extraction from the CB of $TiO_2$ to the external circuit, resulting in unproductive leakage current pathways and overall, an underestimation of the counted charges.[53] This was confirmed through applying a more positive

potential during CPPEs resulting in FE ~100%, whereas bringing the applied potential closer to $E_{CB}(TiO_2)$ delivered abnormally high FEs (Supplementary Figure 27 and Supplementary Table 13).

We then constructed the semi-artificial PEC cell by connecting the two electrodes in a two-compartment cell, separated by a Nafion membrane, with the 4-MBA substrate only in the photoanode compartment. Irradiation of the photoanode led to a net photocurrent at zero applied voltage ($U_{app}$ = 0.0 V) (**Error! Reference source not found.**b) during the LSV measurement. CPPE experiments under these bias-free conditions resulted in a stable photocurrent of 30 µA $cm^{-2}$ over the course of 6 h of irradiation (**Error! Reference source not found.**c). Analysis of liquid products revealed production of 3.17 ± 0.31 and 2.16 ± 0.26 µmol $cm^{-2}$ of 4-MBAd and formate, formed with a FE of (108 ± 18)% and (74 ± 17)%, respectively (Supplementary Table 14). The high FE for 4-MBAd synthesis is attributed to the inefficient electron extraction explained above, which alongside inaccuracies in formate quantification due to the detection limit of the apparatus, account for the observed higher ratio of 4-MBAd to formate. A conservative calculation of TON values, in which all the dropcast enzymes and immobilised **STEMPO** molecules are assumed to be electrochemically active, leads to a $TON_{FDH}$ of 10,372 ± 1272 and $TON_{\mathbf{STEMPO}}$ = 18 ± 3, highlighting the high efficiency of biological systems in comparison to synthetic catalysts.

We performed control experiments by omitting the molecular components in both compartments (Supplementary Figure 28) in an otherwise complete $mTiO_2$|**STEMPO**/**DPP-CA** || mITO|FDH assembly. Employing a bare $mTiO_2$ electrode as photoanode led to a negligible photocurrent, while the use of a bare mITO electrode cathode resulted in lower photocurrents than the fully assembled cell, with no formate production (Supplementary Table 15). This unproductive photocurrent is attributed to electron accumulation in the metal oxide cathode and proton reduction, and has previously been observed for analogous systems.[54] Although sampling of the headspace revealed no $H_2$ present, the low amounts of gas produced would have largely remained dissolved in the liquid phase.[55]

We investigated the two-electrode cell for HMF oxidation in $NaHCO_3$ buffer (0.2 M, pH 7). As explored above (**Error! Reference source not found.**d), the use of more alkaline conditions

would have benefitted the activity of the photoanode. However, the lower activity of FDH at much higher pH values and ionic strength,[33] as a result of the increase of bicarbonate concentration at higher pH values,[1] required a compromise when selecting the electrolyte. Separate three-electrode experiments for the individual electrodes revealed that both assemblies were able to sustain stable (photo)currents at the potential where a current matching was observed (Supplementary Figure 29 and Supplementary Table 16). Thus, a bias-free two-electrode cell was capable of delivering a photocurrent of 10 μA $cm^{-2}$ over the course of 6 h irradiation (Supplementary Figure 30), resulting in a $TON_{\mathbf{STEMPO}}$ and $TON_{FDH}$ of 9 ± 2 and 4532 ± 945, respectively (Supplementary Table 17). Based on the bias-free photocurrents of the PEC, the solar-to-fuel efficiency is expected to be lower than that of state-of-the art systems for classical $CO_2$ and water splitting.[56–58] Nonetheless, the reported PEC system provides a proof-of-concept demonstration for the development of future PEC devices for simultaneous chemical synthesis and $CO_2$ reduction employing a (bio)molecular hybrid approach based on dye-sensitised photoelectrodes. Further improvement of the coupled system through the incorporation of a bipolar membranes, allowing the conditions in each compartment to be optimised independently,[59] would increase the versatility and activity of this cell configuration. Advances on protein engineering and its local environment may further prolong the stability, which remains as one of the biggest challenges in systems employing isolated bioelectrocatalysts.[60,61] Alternatively, the replacement of the enzymatic catalyst by microorganisms or more robust synthetic catalysts,[62,63] and developments in dye-sensitised solar cell technology may further enable the improvement of the performance of such paired PEC platform.

To date, coupling of $CO_2$-reducing FDH-based (photo)cathodes to water-oxidising photoanodes has either required an applied bias,[20,54,64–66] or displayed lower reaction rate for $CO_2$ reduction products than reported in this study (Supplementary Tables 14 and 17).[67–69] A PEC cell requiring two photoabsorbers and consisting of a $BiVO_4$ photoanode, and a $TiO_2$-coated $CuFeO_2$ and CuO mixed photoelectrode functionalised with FDH resulted in currents of up to 150 μA $cm^{-2}$, albeit with a modest FE of 34% for formate production under bias-free conditions.[67]

Employing solely a single light absorber requires visible light absorption and sufficient thermodynamic driving force to transport electrons to the enzymatic catalyst. A $BiVO_4$ photoanode

for water oxidation was coupled to a dark FDH-based cathode, but the low driving force provided by the $BiVO_4$ photoanode resulted in minimal photocurrents of 0.1 μA $cm^{-2}$ under bias-free conditions.[68] Although a bare $TiO_2$ photoanode ensures sufficient driving force for $CO_2$ reduction with FDH, the lack of visible-light absorption capabilities and use of electron mediators results in systems with low activity and FE (15%).[69] The reported rate of formate production (Supplementary Tables 14 and 17) also compares favourably with a previously reported PEC cell coupled to a photovoltaic module,[20] whilst employing a single light absorber and producing of a sole oxidation product.

Thus, the high activity and efficiency reported in this study is a direct result of the optimised molecular engineering of the photoanode and the careful selection of the cathode material and biocatalyst. Utilising a dye-sensitised $TiO_2$ photoanode allows for intense visible light absorption by the organic chromophore and sufficient driving force for $CO_2$ reduction provided by the CB of the $TiO_2$ semiconductor. The mITO cathode allows for the electrons to be transferred efficiently from the hybrid photoanode to the adsorbed FDH enzyme through direct electron transfer. Overall, the fully assembled system showcases simultaneous $CO_2$ reduction and substrate oxidation in a PEC-driven cell. The cell is capable of utilising a single light absorber, without the need of an external bias and the use of precious metals, to achieve high photocurrents, FE and stability.

## Conclusions

We report an unbiased precious metal-free PEC cell capable of simultaneous $CO_2$ reduction and chemical synthesis. We first constructed and characterised a dye-sensitised $TiO_2$ photoanode with a co-immobilised organic molecular chromophore and catalyst. We synthesised a series of organic chromophores, which were then coupled to a silatrane-functionalised TEMPO catalyst for alcohol oxidation in aqueous conditions. The system delivered up to 100 μA $cm^{-2}$ for the oxidation of 4-methylbenzyl alcohol to the corresponding aldehyde over the course of 6 h without significant chromophore degradation in sodium borate buffer (pH 8.0). Both organic chromophores outperform a ruthenium-based photoabsorber and allow for the construction of a precious metal-free dye sensitised photoanode for chemical synthesis in aqueous conditions. The electrode delivered photocurrents over the course of up to 22 h of irradiation, resulting in a $TON_{STEMPO}$ and

$TON_{DPP\text{-}CA}$ of 131 and 853, respectively. We then wired the photoanode to a mITO|FDH cathode in a two-electrode fashion, resulting in unbiased $CO_2$ reduction and 4-MBA oxidation over the course of 6 h, while maintaining a high FE for both products. Expansion of the substrate scope to 5(hydroxymethyl)furfural oxidation revealed a high selectivity for 2,5-diformylfuran production and resulted in photocurrents of 10 μA $cm^{-2}$ with simultaneous $CO_2$ reduction. This study shows that through careful selection of the molecular components, single light absorbers can provide sufficient driving force for $CO_2$ reduction and chemical synthesis without the need of applied potentials and precious-metal components.

## Methods

### Materials

Chemicals for synthesis and analytical measurements were of the highest available purity unless otherwise noted: 2,5-diformylfuran (97%, Sigma Aldrich), 4-methylbenzyl alcohol (99%, Alfa Aesar), 4methylbenzyldehyde (97%, Sigma Aldrich), 5-(hydroxymethyl)furfural (98%, ACROS Organics), absolute ethanol (VWR Chemicals), DL-dithiotreithol (DTT, BioXtra >99.5%, Sigma Aldrich), tris(hydroxymethyl)aminomethane hydrochloride (Tris-HCl >99.0%, Sigma Aldrich), formate solution (1 g $L^{-1}$, Sigma Aldrich, ≥ 99.0%), glacial acetic acid (Fisher Chemical). Acetonitrile (MeCN), dichloromethane (DCM), methanol (MeOH), piperidine, tetrahydrofuran (THF) and triethylamine (TEA) were distilled on calcium hydride (TEA, MeOH and DCM), potassium hydroxide (piperidine) or sodium (THF) before use. Dry 1,4-dioxane (99.8%) and dry *N*,*N*-dimethylformamide (DMF, 99.8%) were purchased from Sigma Aldrich.

Column chromatography was carried out with silica gel 60 (0.040–0.063 mm mesh) from Material Harvest. Fluorine-doped tin oxide (FTO)-coated glass sheets ($SnO_2$/F, 7 Ω $sq^{-1}$ sheet resistance, 300 × 300 × 2 mm) and ITO nanopowder (diameter <50 nm; BET = 27 $m^2$ $g^{-1}$; 90% $In_2O_3$, 10% $SnO_2$) were obtained from Sigma Aldrich. The $TiO_2$ paste (15–20 nm, Ti-Nanoxide T/SP, 100% anatase) was purchased from Solaronix. Sodium hydrogen carbonate (>99.998% trace metal basis) was purchased from Puratronic. Ti foil (0.25 mm thick, 99.5% purity) was purchased from

Alfa Aesar. All aqueous solutions were prepared with ultrapure water (deionised water; Milli-Q®, 18.2 MΩ cm).

## Methods for computational calculations

Computations were conducted using Gaussian 09,[70] performing DFT calculations for the ground state and TD-DFT for the excited state.[71] The calculations were adapted from literature protocols, which have been successfully employed for DPP chromophores. Firstly, a rough optimisation of the ground state geometry was performed at the B3LYP/STO3G level with an extra quadratic convergence threshold.[72] The ground state geometry was further optimised at the PBE0/6-311G(d,p) level,[73] via a force-minimisation process using a SCF convergence threshold ($10^{-10}$ a.u.) including a modelling of bulk solvent effects through the polarizable continuum model (PCM) with the permittivity set to DMF.[74] Subsequently, frequency calculations were performed to confirm that the optimised geometry corresponds to an energy minimum. Finally, the first 25 low-lying excited-states were determined using TD-DFT calculations and the CAM-B3LYP/6311+G(2d,p) level of theory,[75] with a tight SCF convergence threshold ($10^{-7}$ a.u.). All plots of computed species were produced with ChemCraft [Chemcraft - graphical software for visualization of quantum chemistry computations. https://www.chemcraftprog.com]. Protons were omitted for clarity. The coordinates of all relevant species are given in Supplementary Tables 1 and 2.

## Electrode preparation

### Preparation of mITO films for chromophore characterisation

Electrodes were prepared as previously described.[29,35] In brief, a dispersion of 20% w/w suspension of commercial ITO nanoparticles (particle size < 50 nm) was prepared in a 5 M acetic acid solution in ethanol , and subsequently spin coated on cleaned FTO-coated glass. The electrodes were then sintered in a Carbolite furnace, and had a geometrical area of approximately 1 × 2 cm and thickness of 3 µm.

### Preparation of $mTiO_2$ films

Electrodes were prepared as previously described.[29,40] In brief, a $mTiO_2$ scaffold was deposited by slot-coating commercial Ti-Nanoxide pastes (15–20 nm particles, 100% anatase, Solaronix) over a defined area (approximately 0.5 × 0.5 cm) on cleaned FTO-coated glass. The electrodes were then sintered in a Carbolite furnace and had an approximate thickness of 6 µm.

### Preparation of mITO films for $CO_2$ reduction

The mITO electrodes for $CO_2$ reduction were prepared from a previously reported procedure.[52] The FTO-coated glass (2 × 1 cm) was sonicated sequentially with isopropanol and ethanol for 30 min and then dried at 180 °C. A scotch tape ring was placed onto the substrate to define the geometrical surface area as 0.19 $cm^2$. The 50 nm ITO nanoparticles (43 mg), synthesised by a previously reported procedure,[52] were dispersed in an acetic acid (57 µL) and ethanol (143 µL) mixture by sonication for >1 h at 45−55 °C in a sealed vial. 5 µL of the cooled ITO suspension was dropcast onto the pre-defined area and after 10 s, spin-coated at 1000 rpm for 30 s. The electrode was allowed to dry for approximately 45 min before the scotch tape was removed. Finally, the electrodes were heated at a rate of 4 °C $min^{-1}$ from room temperature to 400 °C and annealed at this temperature for 1 h. The resulting electrodes had a geometrical surface area of 0.19 $cm^2$ and an average thickness of 8.5 µm.

### Photoelectrode assembly

#### Immobilisation of molecular components

Immobilisation of the catalyst was achieved employing the optimised conditions previously reported for its immobilisation on metal oxide surfaces to ensure fast catalysis kinetics.[14] $mTiO_2$ electrodes were placed in a capped vial and immersed in a solution of **STEMPO** (2 mM) in MeCN (containing 0.2% v/v acetic acid and 0.1% v/v water). The solution was heated to 70 °C for 6 h under a $N_2$ overpressure. After cooling, the $mTiO_2$|**STEMPO** electrodes were rinsed with MeCN, dried under air and stored in the fridge before use.

The chromophores were immobilised in the dark at room temperature. **DPP-CA** was immobilised by immersion of $mTiO_2$|**STEMPO** electrodes in a bath of **DPP-CA** (0.2 mM) in DCM

(2.5 h), DMF (overnight) or MeOH (overnight). **DPP-PA** was immobilised by immersion of $mTiO_2$|**STEMPO** electrodes in a bath of **DPP-PA** (0.2 mM) in DCM overnight. Immobilisation of **RuP** was achieved by immersion of $mTiO_2$|**STEMPO** electrodes in a bath of **RuP** (0.2 mM) in MeOH overnight. The electrodes were then rinsed with the immobilisation solvent, followed by DCM and then dried in air.

**Cathode assembly**

The mITO electrode was wired to a metal rod by attaching copper wire to the electrode using copper tape. The connection was then sealed using successive layers of Teflon tape, parafilm and then a final layer of parafilm over the metal rod and the electrode. Finally, electrical tape was used to cover any bare FTO surface so that only the predefined area was open to the electrolyte solution. W-FDH from *Desulfovibrio vulgaris* Hildenborough was expressed, purified and characterised according to a published method.[33] A 80 mM solution of dithiothreitol (DTT) was made up in Tris-HCl (20 mM, pH 7.6). FDH (1.3 µL, 52 pmol) was incubated with DTT solution (2.5 µL) under inert conditions for 5 min. The FDH-DTT solution was then dropcast onto the mITO electrode and dried for 6 min before cell assembly.

**Photoelectrochemistry**

The sensitised electrodes were wired to a metal rod by attaching copper wire to the electrode using copper tape. The connection was then sealed using layers of Teflon tape and parafilm.

PEC measurements were carried out using an Ivium CompactStat potentiostat in a one-compartment three-necked custom-made cell equipped with a flat borosilicate glass window. A three-electrode setup was used with a Pt counter electrode, a $Ag/AgCl/KCl_{sat}$ reference, and a sensitised electrode as the working electrode. The cell was purged with $N_2$ or $CO_2$ for 15 min prior to the measurements. Unless noted, back illumination was used for all experiments using a calibrated Newport Oriel solar light simulator (150 W, 100 mW $cm^{-2}$ across the solar spectrum, AM 1.5G) fitted with a UQG Optics UV Filter ($\lambda > 420$ nm) and IR water filter. LSVs were conducted at a scan rate of 5 mV $s^{-1}$ with chopped light alternating between dark and light every 5 sec, followed by the chronoamperometry measurement.

The following conversion factor was applied for photoelectrochemical experiments:[76]

$$E_{RHE} = E_{NHE} + (pH \times 0.059) \quad \text{Equation 1}$$

PEC measurements of the two-electrode cell were carried out in a two-compartment two-necked custom-made cell equipped with a flat quartz glass window and separated by a Nafion membrane. The electrolyte employed for both compartments was identical, albeit with the presence of the alcohol substrate in the anodic compartment. A two-electrode setup was used with a $mTiO_2$|**STEMPO**/**DPP-CA** working electrode placed in the compartment featuring the flat quartz glass window, and a mITO|FDH counter electrode placed in the other compartment. A temperature of 25 °C was maintained for all experiments.

**Quantification of molecular components**

The molecular surface coverage of **DPP-CA** was quantified in triplicate using UV–vis spectroscopy following desorption of the chromophore from $mTiO_2$|**DPP-CA** or $mTiO_2$|**STEMPO**/**DPP-CA** electrodes by sonicating in tetrabutylammonium hydroxide 30-hydrate (TBAOH, 0.1 M, DMF, 1−2 mL) for 5 min until the electrode turned colourless. Higher TBAOH concentrations and longer sonication times were avoided to prevent dye decomposition. The absorption maximum at 498 nm was determined and fitted to a calibration curve (conducted in 0.1 M TBAOH in DMF) to determine the loading values.

The molecular surface coverage of **STEMPO** ($\Gamma_{\mathbf{STEMPO}}$) was determined in triplicate by ICP-OES based on Si determination. To minimise background from the glass substrate, $mTiO_2$ films were prepared on Ti foil substrate (Ti|$mTiO_2$). The Ti substrate was cleaned by successive sonication in ethanol and acetone for 15 min each, followed by drying at 70 °C in air before further use. The $mTiO_2$ films were then deposited as described above, affording the Ti|$mTiO_2$ substrates. This was followed by immobilisation of the **STEMPO** catalyst, overnight digestion of the electrodes (*ca.* 0.36 $cm^2$) in aqueous $HNO_3$ (70%, 143 µL) and subsequent dilution to 2% v/v with MilliQ $H_2O$. A background value, obtained in triplicate following digestion of bare Ti|$mTiO_2$ electrodes, was subtracted from the obtained values for Ti|$mTiO_2$|**STEMPO** electrodes. Because of suspected polymerisation of the silatrane moiety, ICP-OES provides an absolute loading of the molecule, but

does not allow for precise quantification of the photoelectrochemically active molecules on the electrode, resulting in a conservative value when calculating TON numbers. The surface coverage of FDH is assumed to be equal the amount of enzyme dropcast onto the electrode surface.

**Product analysis and quantification**

**Gas product analysis**

Measurements for $H_2$ production were performed by manual injection of 50 µL from the headspace of the PEC cell using a gas-tight syringe (Hamilton, GASTIGHT) into a Shimadzu Tracera GC2010 Plus with a barrier discharge ionisation detector (BID). The GC was equipped with a ShinCarbon micro ST column (0.53 mm diameter) kept at 40 °C using helium carrier gas.

**Liquid product analysis and quantification**

After the reaction, a 100 µL aliquot of the solution was taken from the PEC cell and diluted with 900 µL of Milli-Q water and then analysed via high-performance liquid chromatography (HPLC). Substrate conversions and yields were deduced using a Waters 1500-Series HPLC, with an ultraviolet-visible detector (Waters 2489) set at 254 nm and 280 nm for 4-MBA and HMF oxidation, respectively. Conditions for 4-MBA oxidation: samples and standards (15 µL) were injected directly onto a Luna® Omega 3 µm PS C18 100 Å, LC Column 100 × 3.0 mm column purchased from Phenomenex. The mobile phase was comprised of a 1:1 MeCN/$H_2O$ mixture with a total flow rate of 0.5 mL $min^{-1}$ at 40 °C. Conditions for HMF oxidation: samples and standards (15 µL) were injected directly onto a Rezex™ ROA-Organic Acid H+ (8%), LC Column 300 × 7.8 mm column purchased from Phenomenex. The mobile phase was comprised of 2.5 mM sulfuric acid with a total flow rate of 0.5 mL $min^{-1}$ at 60 °C.

When conducting the analysis, 1 h of equilibration was conducted before the first sample injection. Initially, the starting materials and expected main products were analysed separately to identify their respective retention times. This was carried out for 4-MBA and its possible oxidation products: 4-methylbenzaldehyde (4-MBAd) and 4-methylbenzoic acid. Similarly, this process was carried out for HMF and its possible oxidation products: 2,5-diformylfuran (DFF), 2,5-furandicarboxylic acid, 5-formylfuran-2-carboxylic acid and 5-hydroxymethyl-2-furancarboxylic acid

(Supplementary Figure 25). Standard calibration curves of the main product compounds (4-MBAd and DFF) were then produced for product quantification.

Formate production was quantified using ion chromatography (IC) on a Metrohm 882 Compact IC Plus ion chromatograph with a conductivity detector. The eluent buffer was an aqueous solution of $Na_2CO_3$ (3.0 mM) and $NaHCO_3$ (1.0 mM). The system was calibrated for each batch of eluent buffer with samples containing 0.14, 0.28 and 0.42 mM formate in each individual electrolyte. Calibrations were done for each electrolyte batch and the experimental samples matched to the correct calibration batch. Samples were diluted 2-fold with $H_2O$ before injection in the IC.

**Data availability**

The data supporting the findings of the study are available in the paper and its supplementary materials. Source data for the main figures (Figs. 2–4) are provided with the paper. Other source data supporting the findings of this study are available from the Cambridge data repository (https://doi.org/10.17863/CAM.76484)

**Acknowledgements**

The authors acknowledge support from a EPSRC PhD DTA studentship (EP/M508007/1; D. A.-G.), the Christian Doppler Research Association (Austrian Federal Ministry for Digital and Economic Affairs and the National Foundation for Research, Technology and Development) and the OMV Group (M.A.B., J.W. and E.R.), an ERC Consolidator Grant ‘MatEnSAP’ (682833; D.A.G., E.E.M. and E.R.), the Endeavour Scholarship Scheme (M.A.B.), the German National Academy of Sciences Leopoldina for a postdoctoral fellowship (LPDS 2018-04; A.E.), Fundação para a Ciência e Tecnologia (Portugal) for fellowship SFRH/BD/116515/2016 (A.R.O.), grant PTDC/BII-BBF/2050/2020 (I.A.C.P.) and R&D unit MOSTMICRO-ITQB (UIDB/04612/2020 and UIDP/04612/2020). J.W. gratefully acknowledges support from Prof. Roland Fischer and the Deutsche Forschungsgemeinschaft (grant number: FI 502/43-1). We wish to thank Dr Qian Wang, Prof Nikolay Kornienko, Dr Christian Pichler and Dr Andreas Wagner for helpful discussions. We

also thank Dr Nina Heidary and Dr Khoa Ly for their help in preparing the artwork. We appreciate suggestions and comments on the manuscript from Dr Tengfei Li and Dr Qian Wang.

## Author contributions

D.A-G., J.W. and E.R. designed the project. D.A-G. synthesised and characterised the diketopyrrolopyrrole chromophores and the TEMPO-based catalyst. D.A-G. and A.E. performed the DFT calculations and analysed the data. D.A-G. and M.A.B. designed and characterised the alcohol oxidation photoanode, and carried out the photoelectrochemical experiments of the photoanode. E.E.M designed and characterised the $CO_2$ reduction cathode. D.A.-G. and E.E.M carried out the photoelectrochemical experiments of the two-electrode cell, and analysed the data. A.R.O. and I.A.C.P. expressed, purified, and characterised the formate dehydrogenase. D.A.-G., J.W. and E.R. wrote the manuscript with contributions and discussions from all authors. E.R. and J.W. supervised the research work.

## Competing interests

The authors declare no competing interests.

## References

1. Appel, A. M. *et al.* Frontiers, Opportunities, and Challenges in Biochemical and Chemical Catalysis of $CO_2$ Fixation. *Chem. Rev.* **113**, 6621–6658 (2013).
2. Artz, J. *et al.* Sustainable Conversion of Carbon Dioxide: An Integrated Review of Catalysis and Life Cycle Assessment. *Chem. Rev.* **118**, 434–504 (2018).
3. You, B., Liu, X., Jiang, N. & Sun, Y. A General Strategy for Decoupled Hydrogen Production from Water Splitting by Integrating Oxidative Biomass Valorization. *J. Am. Chem. Soc.* **138**, 13639–13646 (2016).
4. Shaner, M. R., Atwater, H. A., Lewis, N. S. & McFarland, E. W. A comparative technoeconomic analysis of renewable hydrogen production using solar energy. *Energy Environ. Sci.* **9**, 2354–2371 (2016).
5. Na, J. *et al.* General technoeconomic analysis for electrochemical coproduction coupling carbon dioxide reduction with organic oxidation. *Nat. Commun.* **10**, 5193 (2019).
6. Reid, L. M., Li, T., Cao, Y. & Berlinguette, C. P. Organic chemistry at anodes and photoanodes. *Sustainable Energy Fuels* **2**, 1905–1927 (2018).
7. Uekert, T., Pichler, C. M., Schubert, T. & Reisner, E. Solar-driven reforming of solid waste for a sustainable future. *Nat. Sustain.* **4**, 383–391 (2021).

8. Rosatella, A. A., Simeonov, S. P., Frade, R. F. M. & Afonso, C. A. M. 5-Hydroxymethylfurfural (HMF) as a building block platform: Biological properties, synthesis and synthetic applications. *Green Chem.* **13**, 754–793 (2011).

9. Wu, Y.-C., Song, R.-J. & Li, J.-H. Recent advances in photoelectrochemical cells (PECs) for organic synthesis. *Org. Chem. Front.* **7**, 1895–1902 (2020).

10. Cha, H. G. & Choi, K.-S. S. Combined biomass valorization and hydrogen production in a photoelectrochemical cell. *Nat Chem* **7**, 328–333 (2015).

11. Li, C., Zhao, X., Wang, A., Huber, G. W. & Zhang, T. Catalytic Transformation of Lignin for the Production of Chemicals and Fuels. *Chem. Rev.* **115**, 11559–11624 (2015).

12. Wang, Y. *et al.* Simultaneous Electrosynthesis of Syngas and an Aldehyde from $CO_2$ and an Alcohol by Molecular Electrocatalysis. *ACS Appl. Energy Mater.* **2**, 97–101 (2019).

13. Li, T., Cao, Y., He, J. & Berlinguette, C. P. Electrolytic $CO_2$ Reduction in Tandem with Oxidative Organic Chemistry. *ACS Cent. Sci.* **3**, 778–783 (2017).

14. Bajada, M. A. *et al.* A Precious-Metal-Free Hybrid Electrolyzer for Alcohol Oxidation Coupled to $CO_2$ -to-Syngas Conversion. *Angew. Chem. Int. Ed.* **59**, 15633–15641 (2020).

15. Wang, L., Zhang, X., Yang, L., Wang, C. & Wang, H. Photocatalytic reduction of $CO_2$ coupled with selective alcohol oxidation under ambient conditions. *Catal. Sci. Technol.* **5**, 4800–4805 (2015).

16. Chen, Y. *et al.* Coupling photocatalytic $CO_2$ reduction with benzyl alcohol oxidation to produce benzyl acetate over $Cu_2O$/Cu. *Catal. Sci. Technol.* **8**, 2218–2223 (2018).

17. Spitler, M. T. *et al.* Practical challenges in the development of photoelectrochemical solar fuels production. *Sustainable Energy Fuels* **4**, 985–995 (2020).

18. Harris, A. W., Yehezkeli, O., Hafenstine, G. R., Goodwin, A. P. & Cha, J. N. Light-Driven Catalytic Upgrading of Butanol in a Biohybrid Photoelectrochemical System. *ACS Sustainable Chem. Eng.* **5**, 8199–8204 (2017).

19. Li, T. *et al.* Photoelectrochemical oxidation of organic substrates in organic media. *Nat. Commun.* **8**, 390 (2017).

20. Wang, D. *et al.* Lignin-fueled photoelectrochemical platform for light-driven redox biotransformation. *Green Chem.* **22**, 5151–5160 (2020).

21. Seabold, J. A. & Choi, K.-S. Effect of a Cobalt-Based Oxygen Evolution Catalyst on the Stability and the Selectivity of Photo-Oxidation Reactions of a $WO_3$ Photoanode. *Chem. Mater.* **23**, 1105–1112 (2011).

22. Bella, F., Gerbaldi, C., Barolo, C. & Grätzel, M. Aqueous dye-sensitized solar cells. *Chem. Soc. Rev.* **44**, 3431–3473 (2015).

23. Grätzel, M. Photoelectrochemical cells. *Nature* **414**, 338–344 (2001).

24. Kavan, L., Tétreault, N., Moehl, T. & Grätzel, M. Electrochemical characterization of $TiO_2$ blocking layers for dye-sensitized solar cells. *J. Phys. Chem. C* **118**, 16408–16418 (2014).

25. Song, W. *et al.* Visible light driven benzyl alcohol dehydrogenation in a dye-sensitized photoelectrosynthesis cell. *J. Am. Chem. Soc.* **136**, 9773–9779 (2014).

26. Pho, T. V. *et al.* Efficient Light-Driven Oxidation of Alcohols Using an Organic Chromophore–Catalyst Assembly Anchored to $TiO_2$. *ACS Appl. Mater. Interfaces* **8**, 9125–9133 (2016).

27. Badgurjar, D. *et al.* Electron-Withdrawing Boron Dipyrromethene Dyes As Visible Light Absorber/Sensitizers on Semiconductor Oxide Surfaces. *ACS Appl. Mater. Interfaces* **12**, 7768–7776 (2020).

28. Creissen, C. E., Warnan, J. & Reisner, E. Solar $H_2$ generation in water with a $CuCrO_2$ photocathode modified with an organic dye and molecular Ni catalyst. *Chem. Sci.* **9**, 1439–1447 (2018).

29. Antón-García, D., Warnan, J. & Reisner, E. A diketopyrrolopyrrole dye-based dyad on a porous $TiO_2$ photoanode for solar-driven water oxidation. *Chem. Sci.* **11**, 12769–12776 (2020).

30. Brennaman, M. K. *et al.* Finding the Way to Solar Fuels with Dye-Sensitized Photoelectrosynthesis Cells. *J. Am. Chem. Soc.* **138**, 13085–13102 (2016).

31. Sokol, K. P. *et al.* Bias-free photoelectrochemical water splitting with photosystem II on a dye-sensitized photoanode wired to hydrogenase. *Nat. Energy* **3**, 944–951 (2018).

32. Miller, M. *et al.* Interfacing Formate Dehydrogenase with Metal Oxides for the Reversible Electrocatalysis and Solar-Driven Reduction of Carbon Dioxide. *Angew. Chem. Int. Ed.* **58**, 4601–4605 (2019).

33. Oliveira, A. R. *et al.* Toward the Mechanistic Understanding of Enzymatic $CO_2$ Reduction. *ACS Catal.* **10**, 3844–3856 (2020).

34. Warnan, J. *et al.* A compact diketopyrrolopyrrole dye as efficient sensitizer in titanium dioxide dye-sensitized solar cells. *J. Photochem. Photobiol, A* **226**, 9–15 (2011).

35. Leung, J. J. *et al.* Solar-driven reduction of aqueous $CO_2$ with a cobalt bis(terpyridine)-based photocathode. *Nat. Catal.* **2**, 354–365 (2019).

36. Hoertz, P. G., Chen, Z., Kent, C. A. & Meyer, T. J. Application of high surface area tin-doped indium oxide nanoparticle films as transparent conducting electrodes. *Inorg. Chem.* **49**, 8179–8181 (2010).

37. Zigler, D. F. *et al.* Disentangling the Physical Processes Responsible for the Kinetic Complexity in Interfacial Electron Transfer of Excited Ru(II) Polypyridyl Dyes on TiO2. *J. Am. Chem. Soc.* **138**, 4426–4438 (2016).

38. Xu, P., McCool, N. S. & Mallouk, T. E. Water splitting dye-sensitized solar cells. *Nano Today* **14**, 42–58 (2017).

39. Willkomm, J. *et al.* Dye-sensitised semiconductors modified with molecular catalysts for light-driven H2 production. *Chem. Soc. Rev.* **45**, 9–23 (2016).

40. Leung, J. J. *et al.* Photoelectrocatalytic $H_2$ evolution in water with molecular catalysts immobilised on p-Si: Via a stabilising mesoporous $TiO_2$ interlayer. *Chem. Sci.* **8**, 5172–5180 (2017).

41. Schreier, M. *et al.* Covalent Immobilization of a Molecular Catalyst on $Cu_2O$ Photocathodes for $CO_2$ Reduction. *J. Am. Chem. Soc.* **138**, 1938–1946 (2016).

42. Kay, A. & Grätzel, M. Artificial photosynthesis. 1. Photosensitization of titania solar cells with chlorophyll derivatives and related natural porphyrins. *J. Phys. Chem.* **97**, 6272–6277 (1993).

43. Manthou, V. S., Pefkianakis, E. K., Falaras, P. & Vougioukalakis, G. C. Co-Adsorbents: A Key Component in Efficient and Robust Dye-Sensitized Solar Cells. *ChemSusChem* **8**, 588–599 (2015).

44. Bruggeman, D. F., Bakker, T. M. A., Mathew, S. & Reek, J. N. H. Redox-Mediated Alcohol Oxidation Coupled to Hydrogen Gas Formation in a Dye-Sensitized Photosynthesis Cell. *Chem. – A Eur. J.* chem.202003306 (2020) doi:10.1002/chem.202003306.

45. Bullock, R. M., Das, A. K. & Appel, A. M. Surface Immobilization of Molecular Electrocatalysts for Energy Conversion. *Chem. Eur. J.* **23**, 7626–7641 (2017).

46. Wang, D. *et al.* Stabilized photoanodes for water oxidation by integration of organic dyes,

water oxidation catalysts, and electron-transfer mediators. *Proc. Natl. Acad. Sci. U. S. A.* **115**, 8523–8528 (2018).

47. Suryani, O. *et al.* A near-infrared organic photosensitizer for use in dye-sensitized photoelectrochemical water splitting. *Chem. Commun.* **53**, 6784–6787 (2017).

48. Yamamoto, M. *et al.* Visible light-driven water oxidation with a subporphyrin sensitizer and a water oxidation catalyst. *Chem. Commun.* **52**, 13702–13705 (2016).

49. Chadderdon, X. H., Chadderdon, D. J., Pfennig, T., Shanks, B. H. & Li, W. Paired electrocatalytic hydrogenation and oxidation of 5-(hydroxymethyl)furfural for efficient production of biomass-derived monomers. *Green Chem.* **21**, 6210–6219 (2019).

50. Kashparova, V. P. *et al.* Selective Synthesis of 2,5-Diformylfuran by Sustainable 4-acetamido-TEMPO/Halogen-Mediated Electrooxidation of 5-Hydroxymethylfurfural. *Chem Asian J.* **11**, 2578–2585 (2016).

51. Rafiee, M., Konz, Z. M., Graaf, M. D., Koolman, H. F. & Stahl, S. S. Electrochemical Oxidation of Alcohols and Aldehydes to Carboxylic Acids Catalyzed by 4-Acetamido-TEMPO: An Alternative to 'anelli' and 'pinnick' Oxidations. *ACS Catal.* **8**, 6738–6744 (2018).

52. Fang, X. *et al.* Structure–Activity Relationships of Hierarchical Three-Dimensional Electrodes with Photosystem II for Semiartificial Photosynthesis. *Nano Lett.* **19**, 1844–1850 (2019).

53. Green, A. N. M., Palomares, E., Haque, S. A., Kroon, J. M. & Durrant, J. R. Charge transport versus recombination in dye-sensitized solar cells employing nanocrystalline TiO2 and SnO2 films. *J. Phys. Chem. B* **109**, 12525–12533 (2005).

54. Sokol, K. P. *et al.* Photoreduction of $CO_2$ with a Formate Dehydrogenase Driven by Photosystem II Using a Semi-artificial Z-Scheme Architecture. *J. Am. Chem. Soc.* **140**, 16418–16422 (2018).

55. Windle, C. D., Massin, J., Chavarot-Kerlidou, M. & Artero, V. A protocol for quantifying hydrogen evolution by dye-sensitized molecular photocathodes and its implementation for evaluating a new covalent architecture based on an optimized dye-catalyst dyad. *Dalton. Trans.* **47**, 10509–10516 (2018).

56. Coridan, R. H. *et al.* Methods for comparing the performance of energy-conversion systems for use in solar fuels and solar electricity generation. *Energy Environ. Sci.* **8**, 2886–2901 (2015).

57. Liu, C., Colón, B. C., Ziesack, M., Silver, P. A. & Nocera, D. G. Water splitting–biosynthetic system with $CO_2$ reduction efficiencies exceeding photosynthesis. *Science* **352**, 1210–1213 (2016).

58. Wang, Q. *et al.* Molecularly engineered photocatalyst sheet for scalable solar formate production from carbon dioxide and water. *Nat. Energy* **5**, 703–710 (2020).

59. Kim, J. H., Hansora, D., Sharma, P., Jang, J.-W. & Lee, J.-S. Toward practical solar hydrogen production-an artificial photosynthetic leaf-to-farm challenge. *Chem. Soc. Rev.* **48**, 1908–1971 (2019).

60. Chen, H. *et al.* Fundamentals, Applications, and Future Directions of Bioelectrocatalysis. *Chem. Rev.* **120**, 12903–12993 (2020).

61. Plumeré, N. *et al.* A redox hydrogel protects hydrogenase from high-potential deactivation and oxygen damage. *Nat. Chem.* **6**, 822–827 (2014).

62. Dalle, K. E. *et al.* Electro- and Solar-Driven Fuel Synthesis with First Row Transition Metal Complexes. *Chem. Rev.* **119**, 2752–2875 (2019).

63. Kornienko, N., Zhang, J. Z., Sakimoto, K. K., Yang, P. & Reisner, E. Interfacing nature's

catalytic machinery with synthetic materials for semi-artificial photosynthesis. *Nat. Nanotechnol.* **13**, 890–899 (2018).

64. Son, E. J. *et al.* Sunlight-assisted, biocatalytic formate synthesis from $CO_2$ and water using silicon-based photoelectrochemical cells. *Chem. Commun.* **52**, 9723–9726 (2016).

65. Kuk, S. K. *et al.* Photoelectrochemical Reduction of Carbon Dioxide to Methanol through a Highly Efficient Enzyme Cascade. *Angew. Chem. Int. Ed.* **56**, 3827–3832 (2017).

66. Nam, D. H. *et al.* Enzymatic photosynthesis of formate from carbon dioxide coupled with highly efficient photoelectrochemical regeneration of nicotinamide cofactors†. *Green Chem.* **18**, 5989–5993 (2016).

67. Kuk, S. K. *et al.* $CO_2$-Reductive, Copper Oxide-Based Photobiocathode for Z-Scheme Semi-Artificial Leaf Structure. *ChemSusChem* **13**, 2940–2944 (2020).

68. Lee, S. Y., Lim, S. Y., Seo, D., Lee, J.-Y. & Chung, T. D. Light-Driven Highly Selective Conversion of $CO_2$ to Formate by Electrosynthesized Enzyme/Cofactor Thin Film Electrode. *Adv. Energy Mater.* **6**, 1502207 (2016).

69. Ishibashi, T., Higashi, M., Ikeda, S. & Amao, Y. Photoelectrochemical $CO_2$ Reduction to Formate with the Sacrificial Reagent Free System of Semiconductor Photocatalysts and Formate Dehydrogenase. *ChemCatChem* **11**, 6227–6235 (2019).

70. Farré, Y. *et al.* Second Generation of Diketopyrrolopyrrole Dyes for NiO-Based Dye-Sensitized Solar Cells. *J. Phys. Chem. C* **120**, 7923–7940 (2016).

71. Frisch, M. J. *et al.* Gaussian 09. Revision D.01, Gaussian Inc, Wallington CT, 2013.

72. Hehre, W. J., Stewart, R. F. & Pople, J. A. Self-consistent molecular-orbital methods. I. Use of gaussian expansions of slater-type atomic orbitals. *J. Chem. Phys.* **51**, 2657–2664 (1969).

73. Adamo, C. & Barone, V. Toward reliable density functional methods without adjustable parameters: The PBE0 model. *J. Chem. Phys.* **110**, 6158–6170 (1999).

74. Tomasi, J., Mennucci, B. & Cammi, R. Quantum mechanical continuum solvation models. *Chem. Rev.* **105**, 2999–3093 (2005).

75. Yanai, T., Tew, D. P. & Handy, N. C. A new hybrid exchange-correlation functional using the Coulomb-attenuating method (CAM-B3LYP). *Chem. Phys. Lett.* **393**, 51–57 (2004).

76. Sawyer, D. T., Sobkowiak, A. & Roberts, J. L. *Electrochemistry for Chemists*. (Wiley-Interscience, 1995).

## Figures and captions

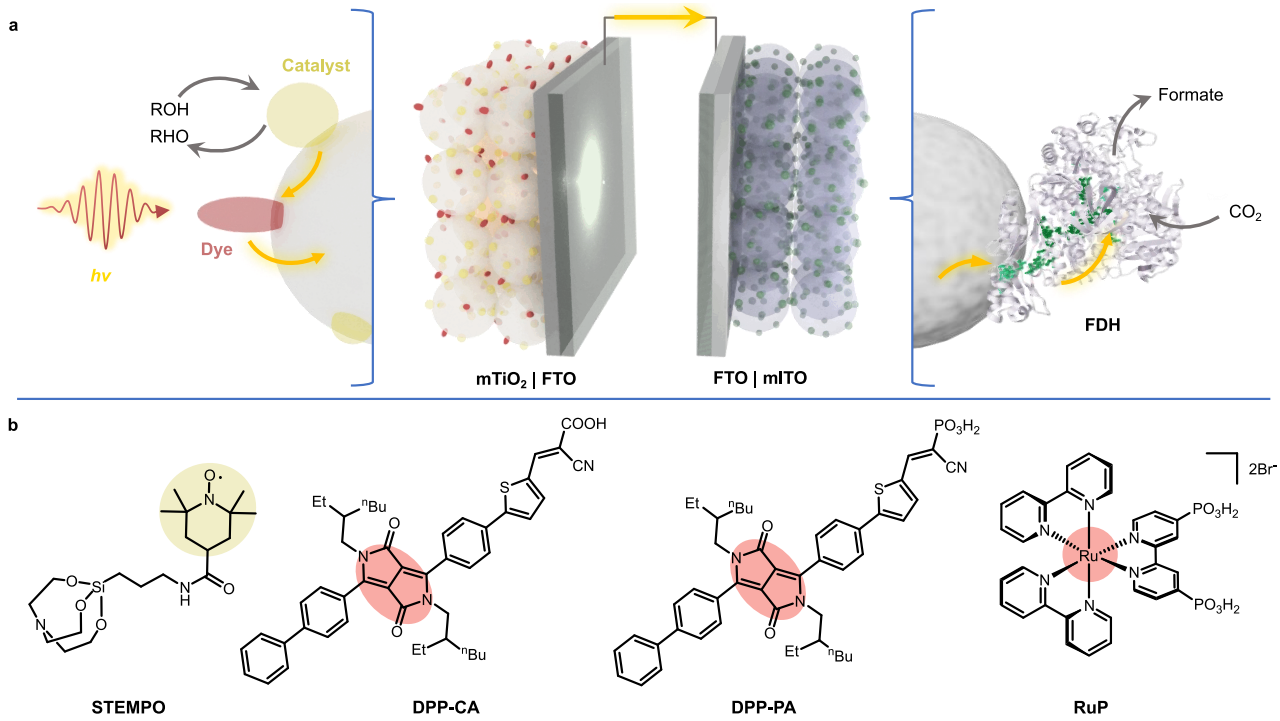


**Figure 1.** PEC cell with molecular components. (a) Schematic representation of the fully-assembled two-electrode cell. Orange arrows indicate electron flow. (b) Structures of synthesised catalyst (yellow) and dyes (red) used in the photoanode study.

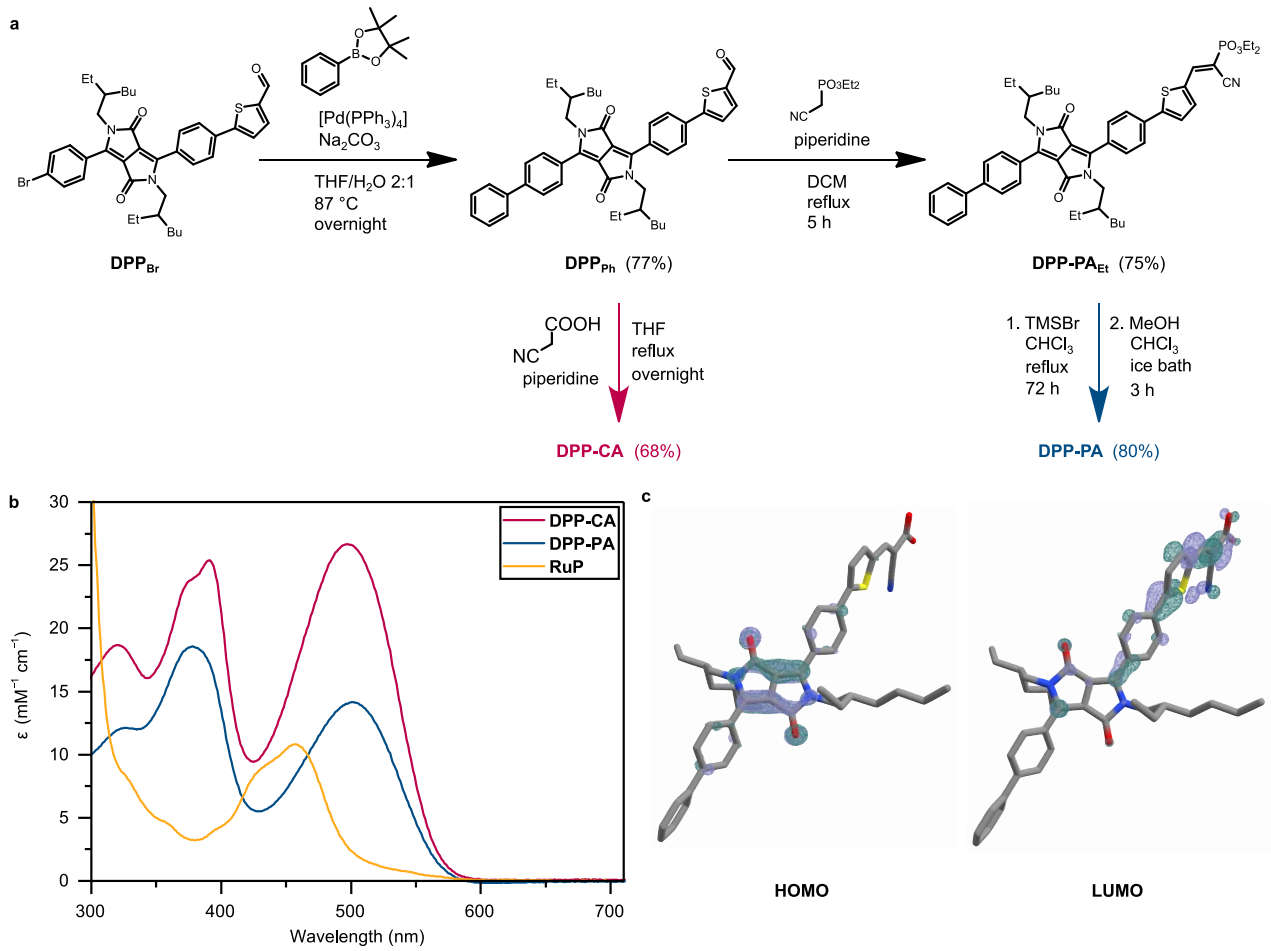


**Figure 2.** Synthesis and characterisation of the dyes. (a) Synthetic route to **DPP-CA** and **DPP-PA**. (b) UV-vis absorption spectra of **DPP-CA**, **DPP-PA** and **RuP** in DMF solution. (c) Frontier molecular orbitals of **DPP-CA**.

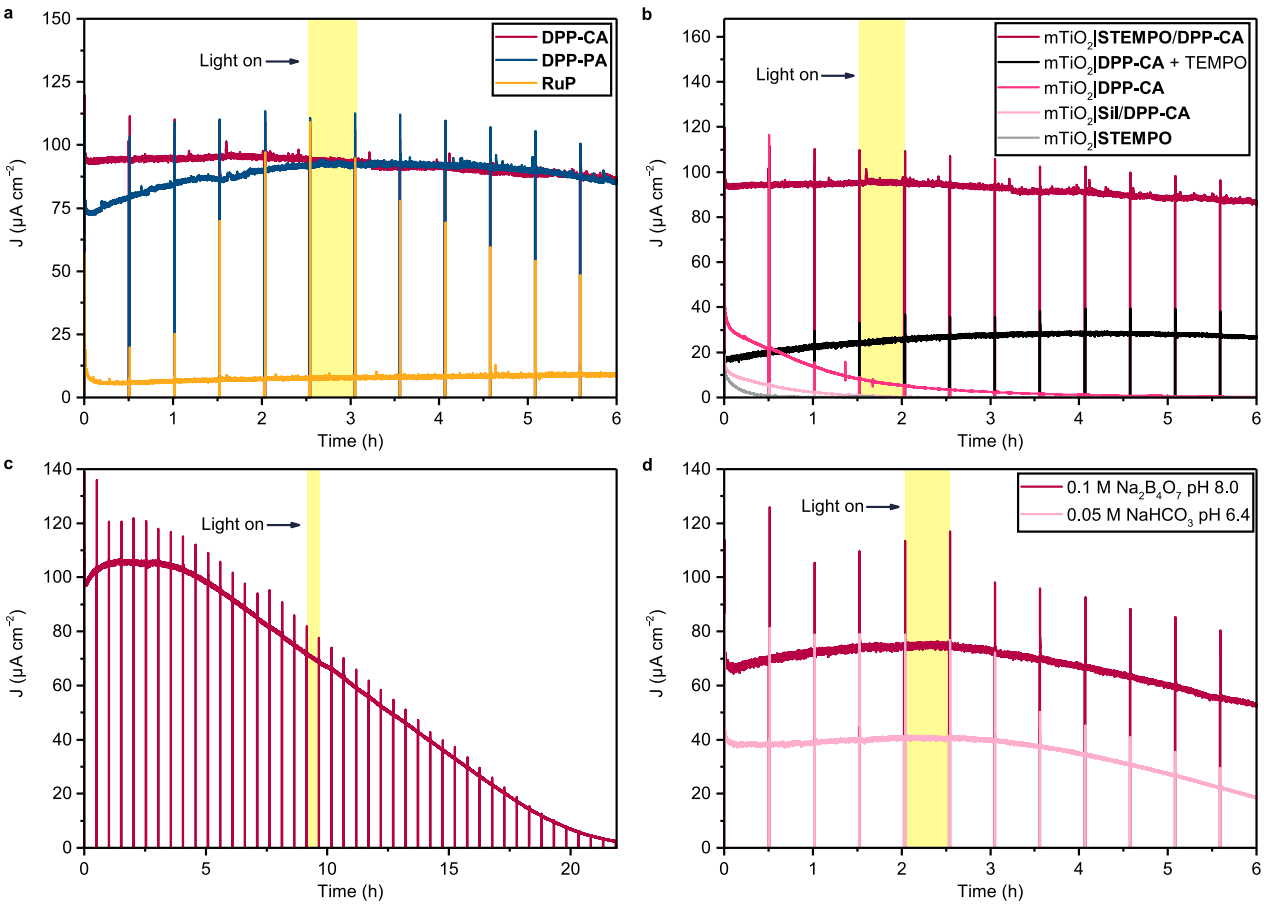


**Fig. 3:** PEC characterisation of the photoanode. (a) Comparison of $mTiO_2$|**STEMPO**/dye electrodes for 4-MBA oxidation in $Na_2B_4O_7$ buffer (0.1 M, pH 8.0, **DPP-CA** and **DPP-PA**) or NaOAc buffer (0.1 M, pH 5.6, **RuP**). (b) Control experiments for $mTiO_2$-based electrodes for 4-MBA oxidation. (c) Long term experiment of a $mTiO_2$|**STEMPO**/**DPP-CA** electrode for 4-MBA oxidation. (d) HMF oxidation with $mTiO_2$|**STEMPO**/**DPP-CA** electrodes. Conditions: $E_{app}$ = +0.4 V *vs.* RHE, 10 mM 4-MBA or 30 mM HMF, 1 mM TEMPO for solubilised catalyst experiment, $N_2$-purged $Na_2B_4O_7$ buffer (0.1 M, pH 8.0) or $CO_2$-purged $NaHCO_3$ buffer (0.05 M, pH 6.4), 100 mW cm$^{-2}$, AM 1.5G, λ > 420 nm, room temperature.

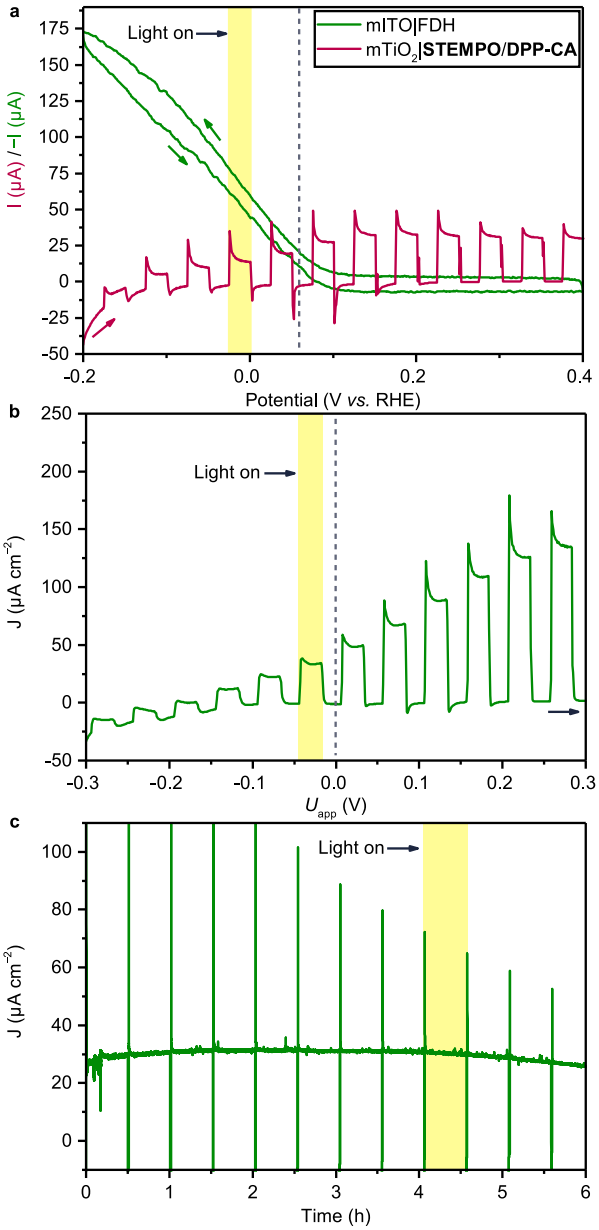


**Fig. 4:** Simultaneous $CO_2$ reduction and 4-MBA oxidation in a two-electrode $mTiO_2$|**STEMPO/DPP-CA** || mITO|FDH PEC cell. (a) Three-electrode LSV of $mTiO_2$|**STEMPO/DPP-CA** (0.25 $cm^2$) and cyclic voltammogram of mITO|FDH (0.19 $cm^2$), under chopped light illumination at the photoanode ($v$ = 5 mV $s^{-1}$). Dashed line highlights current matching potential. (b) LSV of the two-electrode cell under chopped light illumination ($v$ = 5 mV $s^{-1}$). Dashed line highlights zero V applied voltage. (c) CPPE of the two-electrode cell at zero V applied voltage. Conditions: 10 mM 4-MBA (photoanode), $NaHCO_3$ buffer (0.05 M, pH 6.4), 100 mW $cm^{-2}$, AM 1.5G, λ > 420 nm, $CO_2$-purged, 25 °C.